Journal of Solid State Chemistry 183 (2010) 575–583

Contents lists available at ScienceDirect

Journal of Solid State Chemistry

journal homepage: www.elsevier.com/locate/jssc

Synthesis, crystal structures and photoluminescent properties of lanthanide supramolecular complexes with 4-oxo-1(4H)-quinolineacetate

Jun Wang, Jun Fan *, LiangYu Guo, Xia Yin, ZhiHong Wang, WeiGuang Zhang *

School of Chemistry and Environment, South China Normal University, Guangzhou 510006, PR China

ARTICLE INFO

Article history:
Received 30 September 2009
Received in revised form
13 December 2009
Accepted 27 December 2009
Available online 4 January 2010

Keywords:
Lanthanide
4-Oxo-1(4H)-quinolineacetate
Supramolecular network
Luminescence

ABSTRACT

Five new lanthanide supramolecular complexes, namely, $[Sm(oqa)_2(H_2O)_4]_2$ $(ClO_4)_2\cdot(bpy)_2$ (1), $[Ln(oqa)_3]\cdot 2H_2O$ [*Ln*=Sm(**2**), Gd(**3**)] and $[Ln(oqa)_2(NO_3)(H_2O)]$ [*Ln*=Pr(**4**), Eu(**5**)] (oqa=4-oxo-1(4H)-quinolineacetate, bpy=4,4′-bipyridine), have been synthesized under hydrothermal conditions. These complexes exhibit three typical structure features. Complex **1** possesses a dimeric structure, which is further connected together through hydrogen bonds and π–π attractions, forming a 3D supramolecular framework. Compounds **2**–**3** are isomorphous and contain 1D ring-like chains, which are further interconnected by the oqa ligands into 2D sheet-like structures. **4** and **5** exhibit eight-connected 3D network of $4^{24}\cdot 6^4$-*bcu* topology. The various coordination modes of carboxylate ligands and the selection of the counterions have clearly affected the topological structures. Furthermore, the solid-state luminescent properties of complexes **1**, **2** and **5** were investigated at room temperature and they show intense, characteristic emissions in the visible region.

1. Introduction

The rational design and synthesis of lanthanide–carboxylate coordination polymers have attracted considerable attention in the field of supramolecular chemistry and crystal engineering in recent years, due to the fascinating network topologies and promising applications as functional materials [1–7]. In order to obtain lanthanide complexes with different dimensional topological structures, for instance, ladder, brick-wall, layer, honeycomb, non-interpenetrated and interpenetrated 3D networks, etc., a great many carboxylate ligands with rigidity, such as benzene-, pyridine- and pyrazole-multicarboxylates [8–13], have been preferentially selected due to adopting abundant coordination modes. However, only a limited amount of research has been reported by using polycarboxylate ligands combining the characteristic of rigidity and flexibility such as benzene- and quinolyl-oxyacetate [14–16], which will be quite important in generating the coordination polymers with unprecedented network and striking functions. In addition, it is well documented that the choice of the counterions is one of the key factors that has great effect on the topological structures of the complexes. The counterions with weak coordination ability such as ClO_4^-, BF_4^-, SiF_6^{2-}, etc. [17–19] mainly exist in the crystal lattice through electrostatic forces and hydrogen bonds during the process of crystallization. On the contrary, those with strong coordination ability such as NO_3^-, N_3^-, SO_4^{2-}, etc. [20–23] usually act as the favorable donors and even the potential linkers to connect the isolated or low-dimensional coordination units, leading to the formation of the complicated high-dimensional frameworks.

Hydroxyl-substituted quinolines and their derivatives have been already applied in pharmaceutical research [24,25]. Moreover, they have multifunctional coordination sites with chelating and bridging ability in the field of crystal engineering [26,27]. In solid structures, weak interactions such as hydrogen bonds and π–π stacking attractions are often observed. Herein, we present the synthesis, crystal structures and physical properties of lanthanide coordination polymers with 4-oxo-1(4H)-quinolineacetate (oqa) under hydrothermal conditions. We also utilized the counterions such as perchlorate and nitrate to construct unprecedented lanthanide coordination networks.

2. Experimental

2.1. Materials and general methods

The ligand 4-oxo-1(4H)-quinolineacetic acid (Hoqa) was prepared according to the literature [28]. Lanthanide nitrate salts were prepared by dissolving their respective oxides in 1:1 nitric acid (V/V) followed by drying. All the other reagents were commercially available and used without further purification. Elemental (C, H, N) analyses were performed on a Thermo FlashEA112 elemental analyzer. IR spectra were recorded on a

* Corresponding authors. Fax: +86 20 39310187.
E-mail addresses: fanj@scnu.edu.cn (J. Fan), wgzhang@scnu.edu.cn (W. Zhang).

0022-4596/$ - see front matter © 2009 Elsevier Inc. All rights reserved.
doi:10.1016/j.jssc.2009.12.027

Perkin Elmer Spectrum One spectrometer with KBr pellets in the range 4000∼400 cm^{-1}. Thermogravimetric analysis (TGA) experiments were carried out on a Netzsch STA409PC Thermal Analyzer at a heating rate of 10 °C/min up to 800 °C under air atmosphere. Solid-state fluorescent spectra were measured with an Edinburgh FLS920 spectrophotometer at room temperature.

Caution! Perchlorate salts of metal complexes with organic ligands are potentially explosive. They should be handled with care and prepared only in small quantities.

2.2. Syntheses of the compounds

2.2.1. Synthesis of $[Sm(oqa)_2(H_2O)_4]_2(ClO_4)_2$-$(bpy)_2$ (**1**)

A mixture of Sm_2O_3 (0.174 g, 0.50 mmol), Hoqa (0.102 g, 0.50 mmol), 4,4′-bipyridine (0.090 g, 0.50 mmol), $HClO_4$ (0.2 mL) and distilled water (10 mL) was sealed in a 20 mL Teflon-lined stainless-steel reactor and then heated to 120 °C for 48 h under autogenous pressure. After the sample was slowly cooled to room temperature at a rate of 5 °C/h, light-yellow block crystals of **1** were obtained by filtration and washed with water. Yield: 42%. Calcd for $C_{64}H_{64}Cl_2N_8O_{28}Sm_2$ (1764.83): C 43.56, H 3.66, N 6.35; found: C 43.75, H 3.79, N 6.42%. IR (KBr, cm^{-1}): 3198br, 1645s, 1615vs, 1570s, 1489m, 1470w, 1448w, 1405s, 1312s, 1272m, 1242s, 1220m, 1146w, 1108vs, 1062m, 1000w, 807m, 756m, 622m, 593m.

2.2.2. Synthesis of $[Sm(oqa)_3]$-$2H_2O$ (**2**)

A mixture of Sm_2O_3 (0.174 g, 0.50 mmol), Hoqa (0.203 g, 1.0 mmol), $Cu(OAc)_2 \cdot H_2O$ (0.100 g, 0.50 mmol), $HClO_4$ (0.2 mL) and distilled water (10 mL) was sealed in a 20 mL Teflon-lined stainless-steel reactor and then heated to 120 °C for 48 h under autogenous pressure. Light-yellow block crystals of compound **2** were obtained and washed with water. Yield: 35%. Calcd for $C_{33}H_{28}N_3O_{11}Sm$ (792.93): C 49.99, H 3.56, N 5.30; found: C 50.12, H 3.78, N 5.44%. IR (KBr, cm^{-1}): 3514m, 3432m, 1661m, 1637s, 1615vs, 1557vs, 1487s, 1417m, 1376s, 1324 m, 1284m, 1242m, 1212w, 1085w, 1050m, 968w, 932w, 841m, 779s, 593m.

2.2.3. Synthesis of $[Gd(oqa)_3]$-$2H_2O$ (**3**)

Compound **3** was synthesized in a similar procedure as that described in **2**, except that Sm_2O_3 was replaced by Gd_2O_3 (0.180 g, 0.50 mmol). Colorless block crystals of **3** were obtained with a yield of 44%. Calcd for $C_{33}H_{28}GdN_3O_{11}$ (799.83): C 49.55, H 3.53, N 5.25; found: C 49.37, H 3.28, N 5.06%. IR (KBr, cm^{-1}): 3515m, 3429m, 1662m, 1639m, 1616s, 1557vs, 1487s, 1419m, 1378s, 1325m, 1284s, 1241s, 1212m, 1085w, 1050m, 975w, 933m, 841m, 779s, 594m.

2.2.4. Synthesis of $[Pr(oqa)_2(NO_3)(H_2O)]$ (**4**)

A mixture of $Pr(NO_3)_3 \cdot 6H_2O$ (0.435 g, 1.0 mmol), Hoqa (0.102 g, 0.50 mmol), triethylamine (0.2 mL) and H_2O (10 mL) was sealed in a 20 mL Teflon-lined stainless-steel reactor and heated to 120 °C for 48 h under autogenous pressure. Light-green block crystals of **4** were obtained and washed with water. Yield: 52%. Calcd for $C_{22}H_{18}N_3O_{10}Pr$ (625.30): C 42.26, H 2.90, N 6.72; found: C 42.37, H 3.08, N 6.85%. IR (KBr, cm^{-1}): 3429br, 1618vs, 1559vs, 1487s, 1443w, 1412m, 1320m, 1295m, 1282m, 1240s, 1212m, 1184m, 1147m, 1054s, 969m, 923m, 842s, 765s, 587s.

2.2.5. Synthesis of $[Eu(oqa)_2(NO_3)(H_2O)]$ (**5**)

The synthesis of **5** was similar to the above description as **4** except that $Pr(NO_3)_3$ was replaced by $Eu(NO_3)_3$ (0.446 g, 1.0 mmol). Colorless block crystals of **5** were obtained with a yield of 56%. Calcd for $C_{22}H_{18}EuN_3O_{10}$ (636.35): C 41.52, H 2.85, N 6.60; found: C 41.69, H 2.96, N 6.73%. IR (KBr, cm^{-1}): 3402s, 1650m, 1616s, 1567vs, 1495m, 1463m, 1411s, 1312s, 1270w, 1239s, 1208w, 1181m, 1147m, 1058m, 1037s, 971m, 929m, 839s, 761s, 585m.

2.3. X-ray crystallographic analysis

Diffraction data of compounds **1**–**5** were collected on a Bruker APEX II Smart CCD diffractometer equipped with graphite-monochromated Mo*K*α radiation (λ=0.71073 Å) using the ω-scan technique. Multi-scan absorption corrections were applied with the *SADABS* program [29]. The structures were solved by direct methods using the *SHELXS*-97 program and all the non-hydrogen atoms were refined anisotropically with the full-matrix least-squares on F^2 using the *SHELXL*-97 program [30]. The hydrogen atoms of water molecules were located in the difference Fourier maps and the other hydrogen atoms were generated geometrically and refined as riding atoms with isotropic thermal factors. In complex **1**, four oxygen atoms (O7–O10) of perchlorate anion are disordered into two positions with site occupancy factors of 0.463(17) and 0.537(17), respectively. Crystallographic data and structure determination summaries for **1**−**5** are given in Table 1 and the selected bond lengths are listed in Table 2. The hydrogen bonds and selected bond angles for **1**−**5** are listed in Supporting Information, Tables S1 and S2, respectively. CCDC-743545 (**1**), 743546 (**2**), 743547 (**3**), 743548 (**4**) and 743549 (**5**) contain the supplementary crystallographic data for this paper. Copies of these data can be obtained free of charge from The Cambridge Crystallographic Data Centre via www.ccdc.cam.ac.uk/data_request/cif.

3. Results and discussion

3.1. Synthesis

All the compounds **1**–**5** have been synthesized under hydrothermal conditions. These crystalline solids are stable in air and insoluble in water or common organic solvent such as chloroform, ethyl acetate, ethanol and acetone. Scheme 1 summarized the coordination modes of the oqa anion in **1–5**.

For compounds **1**–**3**, lanthanide oxides (Ln_2O_3) were used as the metal sources and adding a small quantity of $HClO_4$ was of advantage to dissolving these oxides and coordinating with the organic ligands. In addition, lanthanide nitrates were selected as the metal sources for **4**–**5** and triethylamine molecules acted as the proton acceptors. The Hoqa molecules were deprotonated after adding some Et_3N, which were confirmed by IR spectra.

In this work, we tried to mix *Ln*(III) ions (*Ln*=Gd, Eu and Sm, etc.) and transition metal ions (Zn^{2+}, Co^{2+} and Cu^{2+}, etc.) with the Hoqa molecules in order to synthesize some 3d–4f bimetallic compounds under hydrothermal conditions. Unfortunately, our efforts failed and only the *Ln*–oqa complexes were obtained in these reaction mixtures, which revealed that the coordination between Ln^{3+} ion and the oqa molecule might have a greater tendency than transition metal ion.

Obviously, some factors such as the starting materials and the pH value of the reaction mixture have greatly influenced their topological structures, indicated by the X-ray crystallography analyses.

3.2. IR spectra

The IR spectra of these compounds show characteristic absorptions for the carboxylate stretching vibrations. The characteristic bands of carboxylate groups are shown in the range

Table 1
Crystallographic data and structure refinement summary for **1**–**5**.

Complex	**1**	**2**	**3**	**4**	**5**
Empirical formula	$C_{64}H_{64}Cl_2N_8O_{28}Sm_2$	$C_{33}H_{28}N_3O_{11}Sm$	$C_{33}H_{28}GdN_3O_{11}$	$C_{22}H_{18}N_3O_{10}Pr$	$C_{22}H_{18}EuN_3O_{10}$
Formula weight	1764.83	792.93	799.83	625.30	636.35
Crystal system	Triclinic	Triclinic	Triclinic	Monoclinic	Monoclinic
Space group	$P-1$	$P-1$	$P-1$	$P\,2_1/c$	$P\,2_1/c$
a (Å)	10.9501(9)	10.275(2)	10.247(2)	12.4600(8)	12.4029(10)
b (Å)	12.8332(10)	11.698(2)	11.672(2)	8.4616(5)	8.4508(7)
c (Å)	13.8212(11)	14.193(3)	14.180(3)	23.4644 (12)	23.2981(16)
α (deg.)	81.0450(12	67.33(2)	67.53(2)	90	90
β (deg.)	67.6650(14)	81.79(2)	82.10(2)	113.762(3)	113.841(3)
γ (deg.)	87.5420(10)	77.89(3)	77.83(3)	90	90
V (Å^3)	1774.3(2)	1535.5(5)	1529.0(6)	2264.2(2)	2233.6(3)
Z	1	2	2	4	4
D_c (g cm^3)	1.652	1.715	1.737	1.834	1.892
μ (mm^{-1})	1.803	1.982	2.239	2.217	2.874
F(000)	886	794	798	1240	1256
Refl. measured	9202	8008	16334	13704	13395
Unique refl. (R_{int})	5796 (0.0183)	5082 (0.0191)	5326 (0.0160)	4252 (0.0347)	4321 (0.0426)
GOF on F^2	1.121	1.054	1.087	1.027	1.038
Final R indices [$I > 2\sigma(I)$]	R_1=0.0317	R_1=0.0239	R_1=0.0312	R=0.0300	R_1=0.0307
	wR_2=0.0856	wR_2=0.0560	wR_2=0.1107	wR_2=0.0621	wR_2=0.0713
R indices (all data)	R_1=0.0355	R_1=0.0265	R_1=0.0335	R_1=0.0408	R_1=0.0396
	wR=0.0888	wR_2=0.0575	wR_2=0.1182	wR_2=0.0657	wR_2=0.0754
Largest diff. peak and hole (e Å^{-3})	1.327,–1.147	0.466,–0.493	0.653,–0.617	0.560,–0.653	1.061,–0.551

[a] $R_1 = \sum ||F_o|-|F_c|| / \sum |F_o|$. [b] $wR_2 = \{\sum[wF_o^2 - F_c^2 / \sum[w(F_o^2)]^2\}^{1/2}$.

Table 2
Selected bonds lengths (Å) for **1**–**5**.

[Sm(4–oqa)$_2$(H$_2$O)$_4$]$_2$(ClO$_4$)$_2$ · (4,4′-bipy) ***(1)***					
Sm(1)–O(1)	2.399(3)	Sm(1)–O(2)#1	2.426(3)	Sm(1)–O(4)	2.586(3)
Sm(1)–O(5)	2.557(3)	Sm(1)–O(5)#1	2.401(3)	Sm(1)–O(1w)	2.446(3)
Sm(1)–O(2w)	2.426(3)	Sm(1)–O(3w)	2.493(3)	Sm(1)–O(4w)	2.488(3)
[Sm(4–oqa)$_3$] · 2H$_2$O ***(2)***					
Sm(1)–O(1)	2.332(2)	Sm(1)–O(3)#1	2.323(3)	Sm(1)–O(4)	2.298(2)
Sm(1)–O(6)#2	2.240(2)	Sm(1)–O(7)	2.336(2)	Sm(1)–O(8)#3	2.587(2)
Sm(1)–O(9)#3	2.504(2)				
[Gd(4 – oqa)$_3$] · 2H$_2$O ***(3)***					
Gd(1)–O(1)	2.318(3)	Gd(1)–O(2)#1	2.487(3)	Gd(1)–O(3)#1	2.566(3)
Gd(1)–O(4)#1	2.314(3)	Gd(1)–O(5)	2.305(3)	Gd(1)–O(7)#2	2.277(4)
Gd(1)–O(9)	2.221(4)				
[Pr(4 – oqa)$_2$(NO$_3$)(H$_2$O)] ***(4)***					
Pr(1)–O(1)	2.393(2)	Pr(1)–O(1w)	2.600(2)	Pr(1)–O(6)	2.436(2)
Pr(1)–O(7)	2.589(2)	Pr(1)–O(8)	2.680(3)	Pr(1)–O(4)#1	2.495(2)
Pr(1)–O(5)#1	2.706(2)	Pr(1)–O(2)#2	2.482(2)	Pr(1)–O(3)#3	2.380(2)
[Eu(4 – oqa)$_2$(NO$_3$)(H$_2$O)] ***(5)***					
Eu(1)–O(1)	2.333(3)	Eu(1)–O(1w)	2.538(3)	Eu(1)–O(6)	2.380(2)
Eu(1)–O(7)	2.535(3)	Eu(1)–O(8)	2.640(4)	Eu(1)–O(4)#1	2.438(3)
Eu(1)–O(5)#1	2.683(3)	Eu(1)–O(2)#2	2.412(2)	Eu(1)–O(3)#3	2.324(3)

Symmetry transformations used to generate equivalent atoms: **1:** #1 2 – x, 1 – y, – z; **2:** #1 – 1 + x, y, z; #2 x, – 1 + y, z; #3 1 + x, y, z; **3:** #1 – 1 + x, y, z; #2 x, – 1 + y, z; **4:** #1 – x, 1/2 + y, 3/2 – z; #2 1 – x, – y, 2 – z; #3 x, 1/2 – y, – 1/2 + z; **5:** #1 2 – x, – 1/2 + y, 3/2 – z; #2 1 – x, 1 – y, 1 – z; #3 x, 1/2 – y, 1/2 + z.

1661–1557 cm^{-1} for asymmetric stretching (ν_{as}) and 1495–1405 cm^{-1} for symmetric stretching (ν_s) [31]. The absence of strong absorption peaks around 1700 cm^{-1} indicates that all carboxyl groups (–COOH) are deprotonated. For complex **1**, the signals at 1146, 1108 and 622 cm^{-1} are the typical stretching vibrations of the free perchlorate anion. For **4** and **5**, the strong peaks in the regions 1487–1463 and 1320–1312 cm^{-1} can be attributed to the characteristic vibrations of the ligated nitrate anions [31]. In addition, the absence of strong absorptions at ca. 1380 cm^{-1} indicates that free NO_3^- anions do not exist in the crystal lattice. Moreover, the strong and broad absorption bands observed in the range 3198–3514 cm^{-1} are due to the presence of water molecules in these compounds.

3.3. Crystal structure descriptions

Complex **1** crystallizes in the triclinic space group $P-1$. X-ray crystallography analysis reveals the formation of the dinuclear complex. As depicted in Fig. 1, each Sm(III) ion is nine-coordinated by five carboxylate oxygen atoms (O1, O2A, O4, O5 and O5A) from four bridging oqa anions and four oxygen atoms (O1w, O2w, O3w and O4w) from four coordinated water molecules, showing a distorted tricapped trigonal prism configuration. The Sm–O bond lengths range from 2.399(3) to 2.557(3) Å, all of which are within the normal ranges [32,33]. In complex **1**, the oqa ligands adopt two kinds of coordination modes: monodentate bridging (Scheme 1a) and bidentate bridging (Scheme 1b). Thus, two Sm(III) ions are connected together with Sm···Sm separation of 4.073(4) Å through the bridging oqa ligands to form a dimeric unit. To balance the charge, free perchlorate anions exist in the crystal lattice through the electrostatic forces. In addition, the bpy molecules are not engaged in coordinating with the Sm(III) ion and occur in the lattice as guest molecules. The nitrogen atoms (N3 and N4) from the bpy molecules and the oxygen atoms (O1w and O2w) from the water molecules form the typical hydrogen bonding interactions [N···O distances, 2.696(6) and 2.813(5) Å, Table S1, Supporting information]. There are also O–H···O hydrogen bonds between the water molecules and the carbonyl oxygen atoms from the oqa ligands [O···O distances, 2.635(5)∼2.798(5) Å, Table S1], resulting in the formation of an extended 2D sheet-like structure (Fig. 2). Moreover, these sheets stack together via π···π interactions between pyridyl groups and quinolyl groups, therefore forming a 3D supramolecular network (Fig. S1).

X-ray diffraction analyses indicate that **2**–**3** are a pair of isomorphous compounds; thus **2** is selected as the representative to be described in detail. Complex **2** exhibits a 2D sheet-like

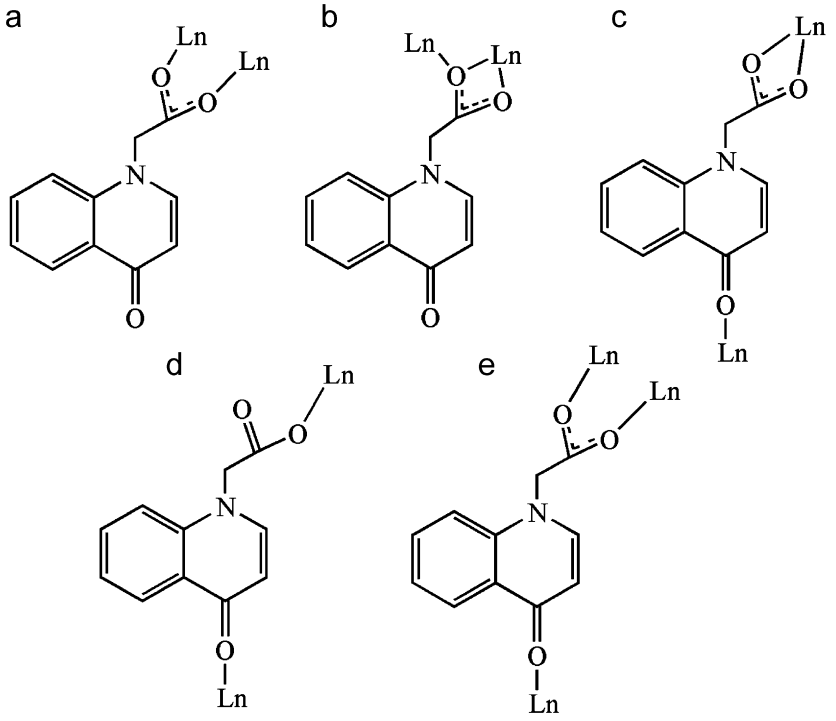

Scheme 1. Coordination modes of the oqa anions in compounds **1**–**5**.

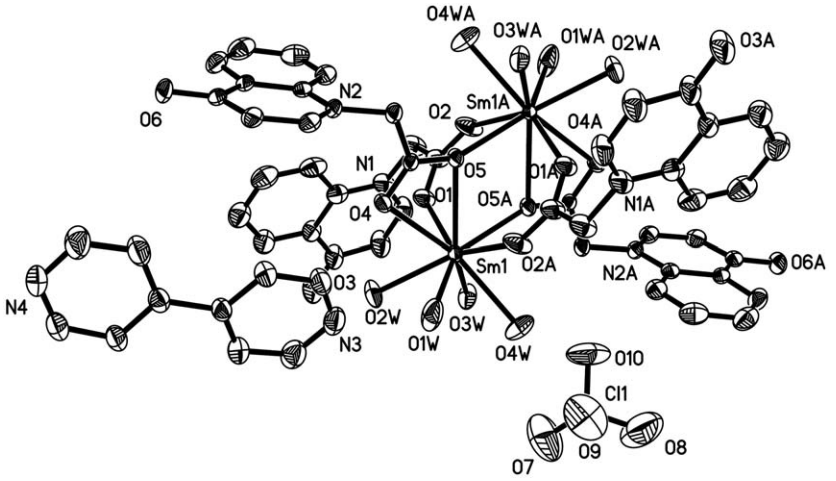

Fig. 1. ORTEP view of **1** with 30% thermal ellipsoids. All hydrogen atoms are omitted for clarity.

structure, crystallizing in a triclinic fashion with space group $P-1$. As illustrated in Fig. 3, each asymmetric unit consists of one Sm(III) ion, three oqa ligands and two lattice water molecules, in which the Sm(III) ion coordinates with seven oxygen atoms from six bridging oqa anions: seven donor atoms form a distorted pentagonal bipyramid configuration. The distances of Sm–O bonds range from 2.240(2) to 2.587(2) Å and the O–Sm–O bond angles are in the range from 50.71(8) to 179.09(10)°, similar to those reported for the Sm(III) complexes [32–33]. In the structure of **2**, three oqa ligands exhibit two kinds of coordination modes: one acts as a μ_2-bridge to connect two Sm(III) ions with the carboxylate group adopting a bidentate chelate mode and the carbonyl oxygen atom adopting a monodentate mode (Scheme 1c); the others also act as μ_2-bridges to link two Sm(III) ions through the carbonyl oxygen atom and the monodentate carboxylate group (Scheme 1d). Further investigation indicates that two adjacent Sm(III) ions are connected together with the separation of Sm⋯Sm (10.275 Å) through two bridging oqa anions, resulting in the formation of a 1D ring-like chain parallel to the *a*-axis (Fig. 4a); then, the adjacent 1D chains are further pillared by the oqa anions (Sm⋯Sm distance, 11.698 Å) along the *b*-axis to generate a 2D sheet-like framework (Fig. 4b). In complex **2**, Sm(III) ions act as the four-connected nodes and the oqa ligands can be described as two-connected rods. On the basis of this simplification, this 2D structure can be described as a (4,4) topological network (Fig. S2). In addition, there are abundant O–H⋯O hydrogen bonds [O⋯O distances, 2.837(4)∼2.883(4) Å] in complex **2** (Table S1). Thus, these 2D layers further extend to a 3D supramolecular network through these hydrogen bonds and π–π packing attraction [centroid–centroid distance =3.419(2) Å] (Fig. S3).

Compounds **4** and **5** are isomorphous, so only complex **4** is chosen as a representative. Complex **4** exhibits an eight-connected 3D framework constructed from dinuclear praseodymium building blocks $[Pr_2(oqa)_4(NO_3)_2(H_2O)_2]$. As shown in Fig. 5,

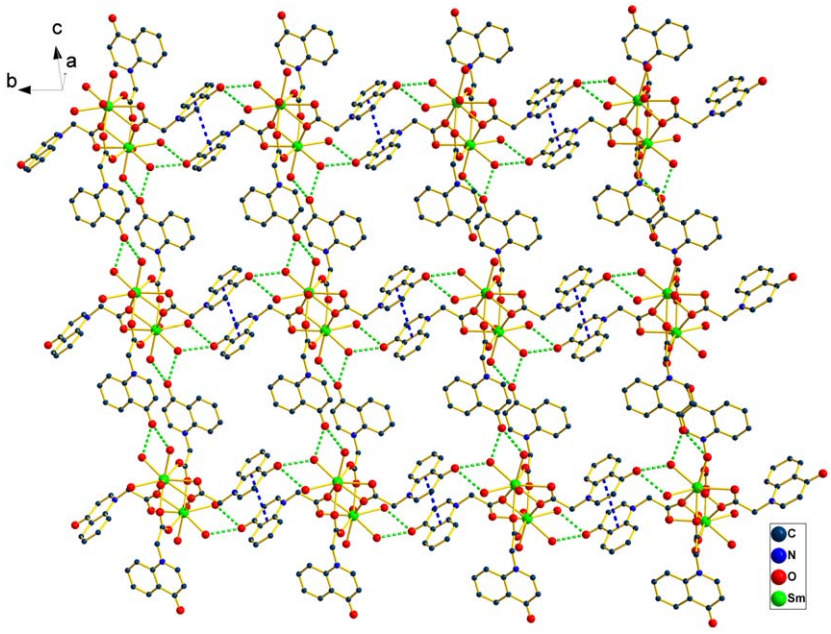

Fig. 2. View of a two-dimensional sheet structure of compound **1**.

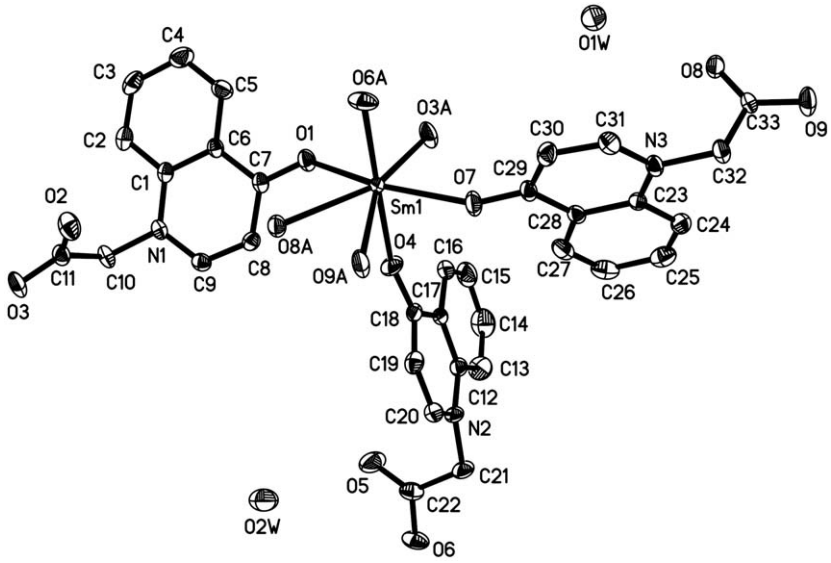

Fig. 3. ORTEP view of **2** with 30% thermal ellipsoids. All hydrogen atoms are omitted for clarity.

the asymmetric unit of **4** contains one crystallographically independent Pr(III) ion, two oqa ligands, one nitrate anion and one ligated water molecule. Each Pr(III) ion is nine-coordinated in an O_9 donor set with the coordination geometry of a distorted tricapped trigonal prism by six oxygen atoms from five bridging oqa ligands, two oxygen atoms from bidentate nitrate and one oxygen atom from the water molecule. The Pr–O bond distances are in the range from 2.380(2) to 2.706(2) Å, all of which are comparable to those reported for the Pr(III) complexes [34, 35]. In complex **4**, the oqa molecules exhibit two kinds of coordination modes: μ_2-bridge (Scheme 1d) and μ_3-bridge (Scheme 1e). Thus, two crystallographically equivalent Pr(III) ions are bridged by the carboxylate groups of the oqa anions to form a dinuclear building block $[Pr_2(oqa)_4(NO_3)_2(H_2O)_2]$ with the Pr···Pr separation of 5.149 Å (Fig. 6a). Then, these dinuclear units are further connected through the bridging oqa anions to generate an extended 3D infinite framework (Fig. 6c). The topological analysis approach was employed to better describe the structure characteristic of **4**. The network topology of the 3D coordination polymer can be simplified by considering the dinuclear Pr(III) building units as the eight-connected nodes and the oqa ligands as two-connected linkers between the cluster nodes. As a result, a 3D network structure of $4^{24}\cdot 6^4$-*bcu* topology decorated by the dinuclear Pr(III) SBUs is formed (Fig. 6d), which corresponds to a bcu topology that is rare for the MOFs [36–43]. To the best of our knowledge, the reactions of *Ln*(III), Mo(IV) and W(IV) ions with potential eight coordination spheres with bridging ligands lead to the construction of eight-connected bcu nets, which may be described as the straightforward approach [36–40]. In addition, utilizing the polynuclear secondary building blocks as the eight-connected nodes such as the formation of compounds **4**–**5** and other reported species [41–43] has been another promising strategy for the bcu net. Moreover, this 3D structure is further stabilized by the rich hydrogen bonds [O···O

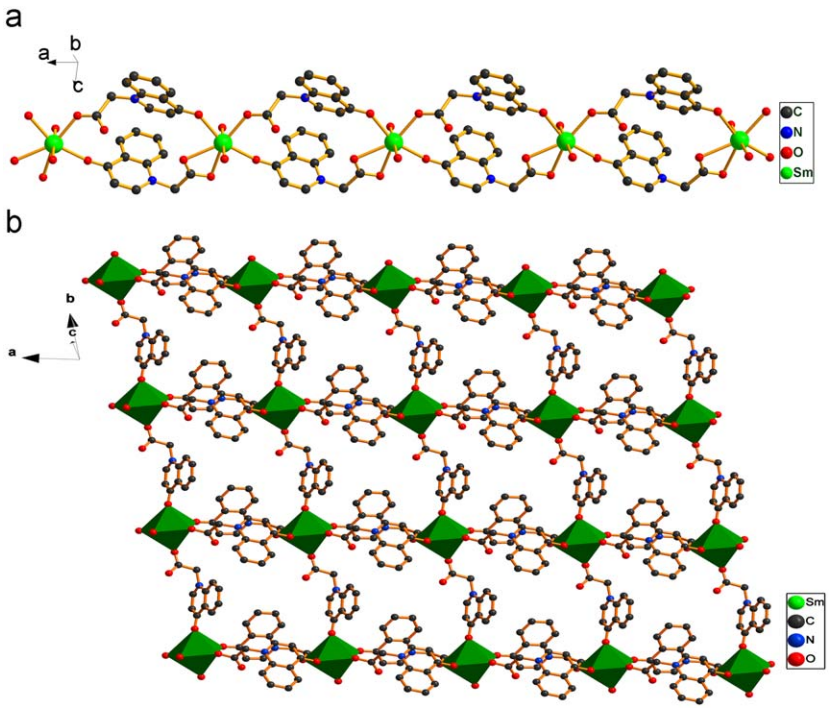

Fig. 4. (a) View of 1D ring-like chain in complex **2** and (b) the 2D layer-like structure constructed by Sm(III) ions and the oqa anions. Lattice water molecules and all hydrogen atoms are omitted for clarity.

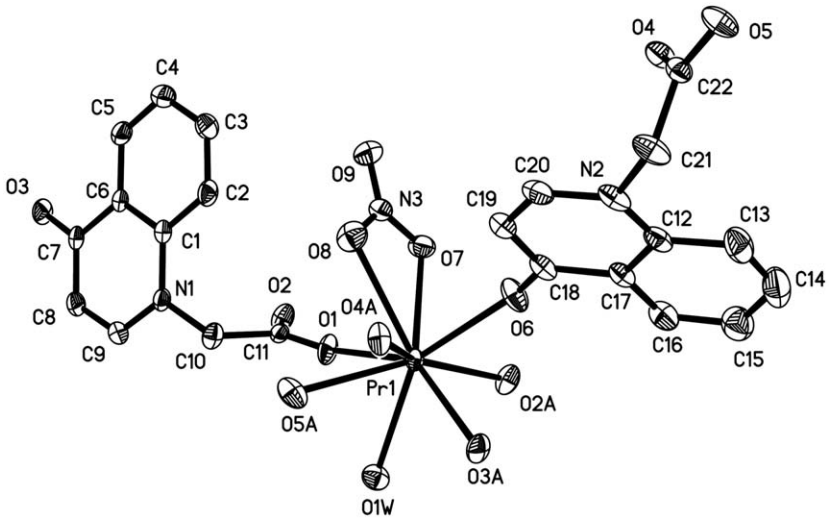

Fig. 5. ORTEP view of **4** with 30% thermal ellipsoids. All hydrogen atoms are omitted for clarity.

distances, 2.910(3)∼2.938(4) Å] (Table S1) and π–π stacking attractions.

For five lanthanide complexes reported in this work, X-ray diffraction studies reveal that they can be classified into three kinds of structure features: a dinuclear structure for **1**, the (4,4)-2D sheet-like networks for **2**–**3** as well as the eight-connected 3D frameworks for **4**–**5**. The possible explanation for this change might be the combination of the versatile coordination behavior of the oqa anion and the choice of the counterion.

The oqa ligands exhibit five kinds of coordination modes in the formation of compounds **1**–**5**. In complex **1**, only the carboxylate oxygen atoms of the oqa ligand take part in the coordination with Sm(III) ions (Scheme 1a, b), whereas the carbonyl oxygen atoms of the oqa ligands do not coordinate with metal ions and act as the hydrogen bonding acceptors to form the strong intermolecular O–H···O hydrogen bonds, resulting in the formation of a 2D sheet. In addition, the free ClO_4^- anions and the bpy molecules exist in the crystal lattice and also act as the acceptors to engage in the formation of O–H···O and O–H···N hydrogen bonds (Table S1), further linking these adjacent 2D sheets to generate a 3D supramolecular framework. For **2**–**3**, no additional counterions are present in the lattice except for the oqa anions. All the oqa anions act as the μ_2-bridges (Scheme 1c, d) through the carboxylate and carbonyl oxygen atoms to connect the adjacent coordination units [Ln(oqa)$_3$] and the 2D sheet is formed by these connection. In **4**–**5**, the nitrate anion exhibits bidentate chelating mode. The eight-connected 3D frameworks are composed of the dinuclear lanthanide building block [Ln_2(oqa)$_4$(NO_3)$_2$(H_2O)$_2$], which are further constructed through the connectivity of carboxylate bridges from the oqa anions.

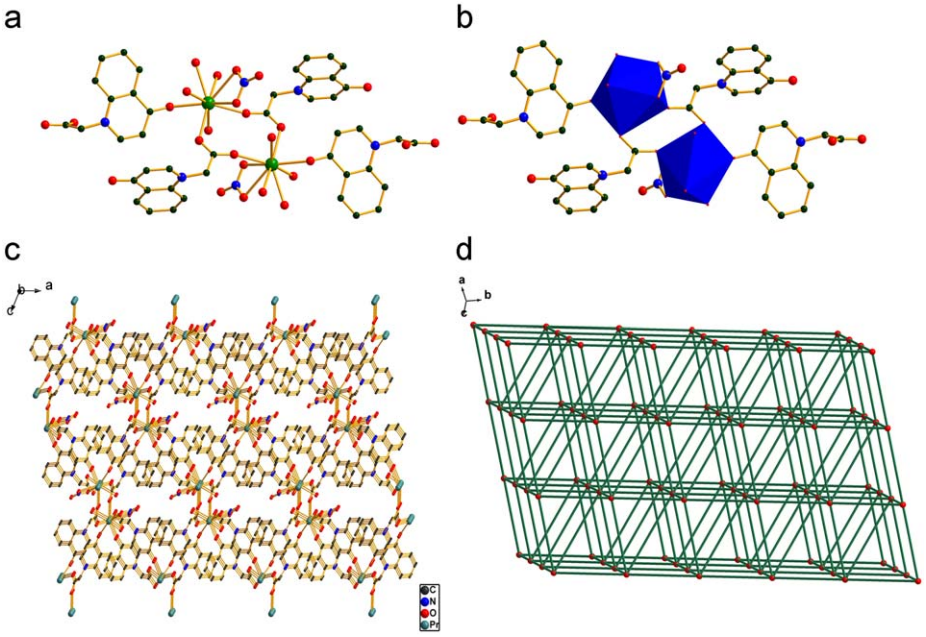

Fig. 6. (a) Ball and stick (b) polyhedral representation of dinuclear building block $[Pr_2(oqa)_4(NO_3)_2(H_2O)_2]$ in **4**. (c) View of a 3D framework in **4**. (d) Schematic representation of the eight-connected framework of **4**.

3.4. Thermal behaviors

Owing to the similarity of the structures for **2**–**3** and **4**–**5**, compounds **3** and **5** were selected for thermogravimetric analyses to examine the thermal stabilities. TGA curves have been obtained under air atmosphere for crystalline samples of **1**, **3** and **5** in the temperature range from 50 to 800 °C (Fig. S4).

The TGA curve of complex **1** displays three obvious steps weight losses. The first weight loss of 7.99% from 90 to 140 °C corresponds to the removal of all the water molecules (calcd: 8.17%) in the asymmetric unit. The second weight loss of 17.22% between 150 and 300 °C is attributable to the loss of the bpy molecules (calcd: 17.69%). The further weight loss above 350 °C is attributable to decomposition of the whole coordination framework. Seen from the TG curve of complex **3**, the first weight loss of 4.01% is ascribed to removal of the water molecules (calcd: 4.54%) below 220 °C. The major weight loss occurs in next step above 315 °C, which may correspond to the collapse of the coordination structure. Above 600 °C, the TGA curve does not change with temperature, suggesting that a residue (Gd_2O_3) has been obtained in 22.90% yield (calcd: 22.67%). For complex **5**, the coordinated water molecule is removed in the temperature range 120–200 °C (calcd/found: 2.88%/3.35%). The decomposition of the coordination framework occurs above 320 °C. The remaining weight of 27.35% corresponds to the percentage (27.65%) of Eu and O components, indicating that the final product may be Eu_2O_3.

Thermal analysis results revealed that the removal of the ligated/free water molecules and the guest molecules was easily observed in the lower temperature, compared with the decomposition of the coordination framework. In addition, the complexes with complicated framework show higher thermal stability than those with low-dimensional structure.

3.5. Photoluminescent properties

Owing to the promising luminescent properties of Eu(III) and Sm(III) ions in the visible region, the solid-state luminescent properties of complexes **1**, **2** and **5** were investigated at room temperature.

The emission spectra of complexes **1** (Fig. 7a, λ_{ex}=345 nm) and **2** (Fig. 7b, λ_{ex}=356 nm) exhibit the characteristic emission of Sm(III) ions in the solid state. The emission at 563, 599, and 646 nm is attributed to the characteristic emission of $^4G_{5/2}\rightarrow{}^6H_J$($J$=5/2, 7/2, 9/2) transition of the Sm^{3+} ion [44]. In complex **2**, the emission at 599 nm from the $^4G_{5/2}\rightarrow{}^6H_{7/2}$ transition is the strongest among these peaks.

As shown in Fig. 7c, compound **5** exhibits an intense, characteristic red emission upon the excitation at 394 nm. The emission bands observed at 578, 589, 615, 651 and 699 nm can be ascribed to be the characteristic emission $^5D_0\rightarrow{}^7F_J$(J=0–4) transition of Eu(III) ion [33]. The dominant band at 615 nm is the hypersensitive $^5D_0\rightarrow{}^7F_2$ transition of Eu(III) ion, which is very sensitive to site symmetry. The intensity of the $^5D_0\rightarrow{}^7F_2$ transition is about 5 times stronger than that of the $^5D_0\rightarrow{}^7F_1$ transition at 589 nm, indicating the absence of an inversion center at the Eu(III) site. In addition, the triple splitting of the $^5D_0\rightarrow{}^7F_1$ transition has also suggested the low symmetry site of the Eu(III) ion. This observation is in good accordance with the result of the crystal structure analysis.

4. Conclusion

In summary, the reactions of 4-oxo-1(4H)-quinolineacetate (oqa) with varied lanthanide ions resulted in the formation of five new lanthanide complexes, namely, $[Sm(oqa)_2(H_2O)_4]_2$-$(ClO_4)_2$-$(bpy)_2$(**1**), $[Ln(oqa)_3]$-$2H_2O$ [Ln=Sm(**2**), Gd(**3**)], $[Ln(oqa)_2(NO_3)(H_2O)]$ [Ln=Pr(**4**), Eu(**5**)]. X-ray crystallography analyses reveal that the coordination modes of the carboxylate ligands and the choice of the counterions could promote different topological structures. These compounds exhibit three typical structure features, such as a dimeric structure (**1**), the 2D sheets (**2**–**3**) and the eight-connected 3D frameworks (**4**–**5**). Moreover, complexes **1**, **2** and **5** at the solid state exhibit strong and characteristic emission of Ln(III) ions in the visible region at room temperature.

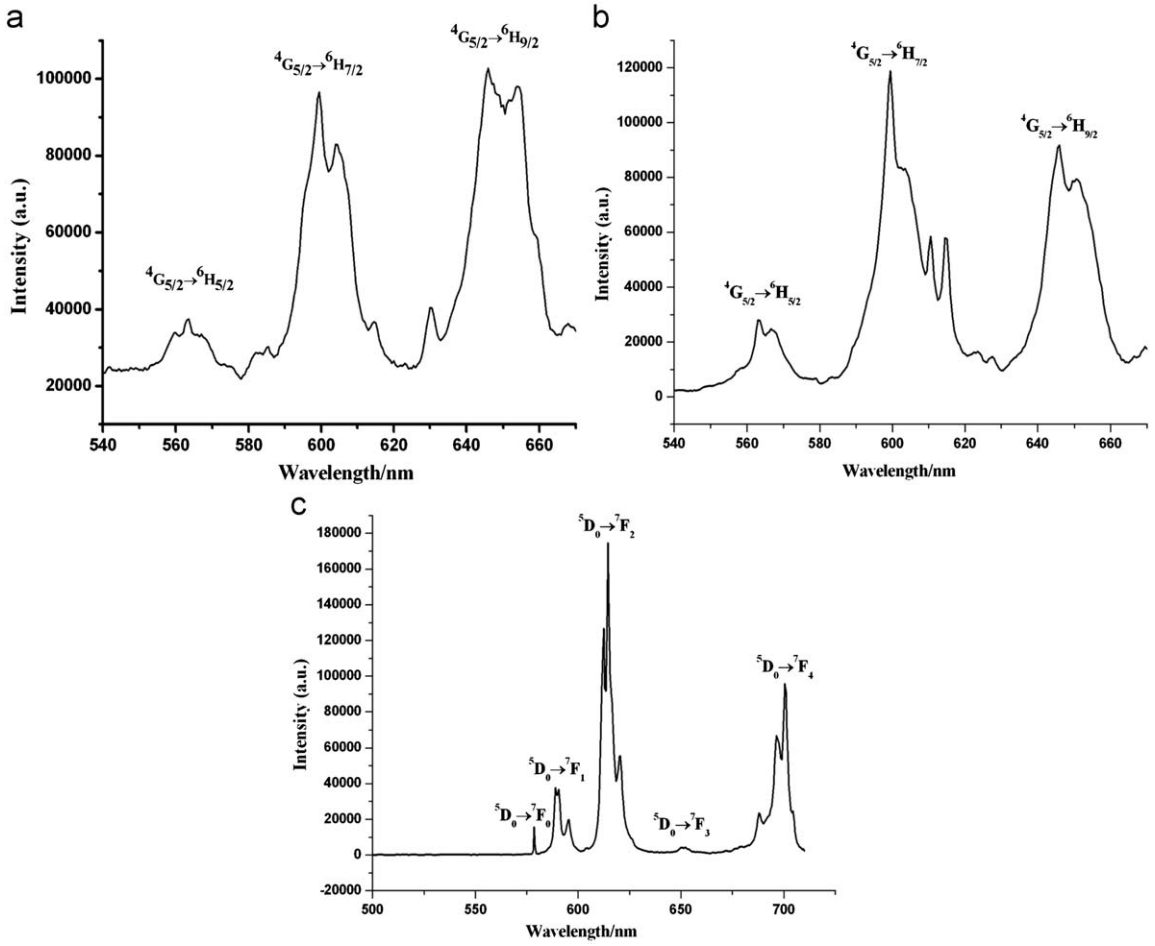

Fig. 7. The solid-state emission spectra of complexes **1** (a, λ_{ex}=345 nm), **2** (b, λ_{ex}=356 nm) and **5** (c, λ_{ex}=394 nm).

Acknowledgment

This work was granted financial support by the National Natural Science Foundation of China (No: 20771040).

Appendix A. Supplementary material

Supplementary data associated with this article can be found in the online version at doi:10.1016/j.jssc.2009.12.027.

References

[1] L. Ma, O.R. Evans, B.M. Foxman, W.B. Lin, Inorg. Chem. 38 (1999) 5837–5840.
[2] J. Inanaga, H. Furuno, T. Hayano, Chem. Rev. 102 (2002) 2211–2225.
[3] J.-P. Costes, J.M. Clemente-Juan, F. Dahan, F. Nicodème, M. Verelst, Angew. Chem. Int. Ed. 41 (2002) 323–325.
[4] P. Lebdušková, P. Hermann, L. Helm, É. Tóth, J. Kotek, K. Binnemans, J. Rudovský, I. Lukeš, A.E. Merbach, Dalton Trans. (2007) 493–501.
[5] T.M. Reineke, M. Eddaoudi, M. Fehr, D. Kelly, O.M. Yaghi, J. Am. Chem. Soc. 121 (1999) 1651–1657.
[6] X.Y. Chen, Y. Bretonnière, J. Pécaut, D. Imbert, J.C.G. Bünzli, M. Mazzanti, Inorg. Chem. 46 (2007) 625–637.
[7] B. Zhao, P. Cheng, X.Y. Chen, C. Cheng, W. Shi, D.Z. Liao, S.P. Yan, Z.H. Jiang, J. Am. Chem. Soc. 126 (2004) 3012–3013.
[8] M.S. Liu, Q.Y. Yu, Y.P. Cai, C.Y. Su, X.M. Lin, X.X. Zhou, J.W. Cai, Cryst. Growth Des. 8 (2008) 4083–4091.
[9] X.J. Gu, D.F. Xue, Cryst. Growth Des. 7 (2007) 1726–1732.
[10] G.L. Law, K.L. Wong, K.K. Lau, H.L. Tam, K.W. Cheah, W.T. Wong, Eur. J. Inorg. Chem. (2007) 5419–5425.
[11] Y.Q. Sun, J. Zhang, Y.M. Chen, G.Y. Yang, Angew. Chem. Int. Ed. 44 (2005) 5814–5817.
[12] D. Bradshaw, J.B. Claridge, E.J. Cussen, T.J. Prior, M.J. Rosseinsky, Acc. Chem. Res. 38 (2005) 273–282.
[13] Y. Huang, B. Yan, M. Shao, J. Solid State Chem. 182 (2009) 657–668.
[14] X.L. Hong, Y.Z. Li, H.M. Hu, Y. Pan, J.F. Bai, X.Z. You, Cryst. Growth Des. 6 (2006) 1221–1226.
[15] X.F. Li, Z.B. Han, X.N. Chen, X.M. Chen, Inorg. Chem. Commun. 9 (2006) 1091–1095.
[16] J. Fan, Z.H. Wang, M. Yang, X. Yin, W.G. Zhang, Z.F. Huang, R.H. Zeng, Cryst. Eng. Comm. 12 (2010) 216–225.
[17] Y. Kataoka, D. Paul, H. Miyake, T. Yaita, E. Miyoshi, H. Mori, S. Tsukamoto, H. Tatewaki, S. Shinoda, H. Tsukube, Chem. Eur. J. 14 (2008) 5258–5266.
[18] J.R. Li, X.H. Bu, R.H. Zhang, C.Y. Duan, K.M.-C. Wong, V.W.W. Yam, New J. Chem. 28 (2004) 261–265.
[19] G. Tavcar, M. Tramsek, T. Bunic, P. Benkic, B. Zemva, J. Fluor. Chem. 125 (2004) 1579–1584.
[20] D.-K. Bucar, G.S. Papaefstathiou, T.D. Hamilton, L.R. MacGillivray, New J. Chem. 32 (2008) 797–799.
[21] S.S. Bao, L.F. Ma, Y. Wang, L. Fang, C.J. Zhu, Y.Z. Li, L.M. Zheng, Chem. Eur. J. 13 (2007) 2333–2343.
[22] S.J. Dalgarno, J.L. Atwood, C.L. Raston, Cryst. Growth Des. 7 (2007) 1762–1770.
[23] E.Q. Gao, Y.F. Yue, S.Q. Bai, Z. He, C.H. Yan, J. Am. Chem. Soc. 126 (2004) 1419–1429.
[24] F.E. Goda, A.A.M. Abdel-Aziz, H.A. Ghoneim, Bioorg. Med. Chem. 13 (2005) 3175–3183.
[25] V. Raja Solomon, W. Haq, K. Srivastava, S.K. Puri, S.B. Katti, J. Med. Chem. 50 (2007) 394–398.
[26] X.N. Cheng, W.X. Zhang, X.M. Chen, J. Am. Chem. Soc. 129 (2007) 15738–15739.
[27] Z.B. Zheng, R.T. Wu, J.K. Li, Y.F. Sun, J. Coord. Chem. 61 (2008) 2750–2759.
[28] M.L. Edwards, R.E. Bambury, H.W. Ritter, J. Med. Chem. 20 (1977) 560–563.
[29] Bruker, SMART and SAINT; Bruker AXS Inc., Madison, Wisconsin, 2004.
[30] G.M. Sheldrick, SHELXS-97 and SHELXL-97, University of Göttingen, Germany, 1997.
[31] K. Nakamoto, Infrared and Raman Spectra of Inorganic and Coordination Compounds, 5th ed., Wiley and Sons, New York, 1997.
[32] Z. He, E.Q. Gao, Z.M. Wang, C.H. Yan, M. Kurmoo, Inorg. Chem. 44 (2005) 862–874.

[33] X.F. Li, Z.L. Xie, J.X. Lin, R. Cao, J. Solid. State Chem. 182 (2009) 2290–2297.
[34] G. Oczko, P. Starynowicz, J. Mol. Struct. 740 (2005) 237–248.
[35] J.W. Ye, J.Y. Zhang, G.L. Ning, G. Tian, Y. Chen, Y. Wang, Cryst. Growth Des. 8 (2008) 3098–3106.
[36] D.L. Long, A.J. Blake, N.R. Champness, C. Wilson, M. Schröder, Angew. Chem. Int. Ed. 40 (2001) 2443–2447.
[37] D.L. Long, R.J. Hill, A.J. Blake, N.R. Champness, P. Hubberstey, D.M. Proserpio, C. Wilson, M. Schröder, Angew. Chem. Int. Ed. 43 (2004) 1851–1854.
[38] R.J. Hill, D.L. Long, P. Hubberstey, M. Schröder, N.R. Champness, J. Solid State Chem. 178 (2005) 2414–2419.
[39] R. Eckhardt, H. Hanika-Heidl, R.D. Fischer, Chem. Eur. J. 9 (2003) 1795–1804.
[40] T.T. Luo, H.L. Tsai, S.L. Yang, Y.H. Liu, R.D. Yadav, C.C. Su, C.H. Ueng, L.G. Lin, K.L. Lu, Angew. Chem. Int. Ed. 44 (2005) 6063–6067.
[41] Q.R. Fang, G.S. Zhu, Z. Jin, M. Xue, X. Wei, D.J. Wang, S.L. Qiu, Angew. Chem. Int. Ed. 45 (2006) 6126–6130.
[42] E.C. Yang, J. Li, B. Ding, Q.Q. Liang, X.G. Wang, X.J. Zhao, Cryst. Eng. Comm. 10 (2008) 158–161.
[43] H.Q. Hao, J. Wang, W.T. Liu, M.L. Tong, Cryst. Eng. Comm. 10 (2008) 1454–1459.
[44] J.W. Cheng, S.T. Zheng, G.Y. Yang, Dalton Trans. (2007) 4059–4066.